Electronic Supporting Information for:

A *p*-type Copper(I)-1,3-Benzenedithiolate 2D Coordination Polymer with High Seebeck Coefficient

Chloé Andrade,[a] Saly Hawila,[a] Ahmad Abdallah,[a] Jean-Luc Rukemampunzi,[a] Adel Mesbah,[a] Nathalie Guillou,[b] Florent Perret,[c] Stefan Wuttke,[d] Thomas Niehaus,[e] Régis Debord,[e] Olivier Boisron,[e] Stéphane Pailhès,[e]* Aude Demessence[a]*

[a]Univ Lyon, Université Claude Bernard Lyon 1, CNRS, Institut de Recherches sur la Catalyse et l'Environnement de Lyon (IRCELYON), UMR CNRS 5256, Villeurbanne, France.

[b]Université Paris-Saclay, UVSQ, CNRS, Institut Lavoisier de Versailles (ILV), UMR 8180, Versailles, France.

[c]Univ Lyon, Université Claude Bernard Lyon 1, CNRS-INSA Lyon-CPE Lyon, Institut de Chimie et de Biochimie Moléculaires et Supramoléculaires (ICBMS), UMR 5246, Villeurbanne, France.

[d]BCMaterials (Basque Center for Materials, Applications & Nanostructures), University of the Basque Country (UPV/EHU), Leioa, Spain. Ikerbasque, Basque Foundation for Science, Bilbao, Spain.

[e]Univ Lyon, Université Claude Bernard Lyon 1, CNRS, Institut Lumière Matière (ILM), UMR 5306, Villeurbanne, France.

stephane.pailhes@univ-lyon1.fr

aude.demessence@ircelyon.univ-lyon1.fr

Experimental and Instrumentation

Chemicals and materials. Copper(I) chloride (CuCl, for analysis) and hydrochloric acid (HCl, 37 % for analysis) were purchased from Merk Germany. Benzene-1,3-dithiol ($C_6H_6S_2$, 99%) was purchased from Sigma Aldrich France. Dimethylformamide (DMF, for HPLC) was purchased from VMR Chemicals. Ethanol was purchased from Carlo Erba Reagents. All reagents and solvents were used as received.

Synthesis of $[Cu_2(1,3\text{-BDT})]_n$. The solution of distilled water (11.5 mL) and hydrochloric acid (1 M, 2.3 mL) is deoxygenated under bubbling of argon for 5 minutes before adding benzene-1,3-dithiol (1.163 mmol, 133 µL). Five minutes later, still under argon stream, copper(I) chloride is added (2.325 mmol, 230 mg). The reaction remained under flow for 5 minutes before being heated to 120 °C for 18 hours on a heat block in a 40 mL sealed glass vial. The product is washed twice with each solvent: distilled water, dimethylformamide and ethanol. 257 mg of a beige product is obtained, i.e. a metal yield of 41 %. Chemical Formula: $C_6H_4S_2Cu_2$. Molecular Weight: 267.3 $g.mol^{-1}$. Copper content from TGA curve (Fig. S2) with Cu_2S as the final product of decomposition, (calc.) wt%: 59.4 (59.5). Elemental analysis: (calc.) wt%: S 23.47 (23.99), H 1.59 (1.51), C 28.42 (26.96).

Characterization techniques.

All the characterizations of the $[Cu_2(1,3\text{-BDT})]_n$ powder or pellets have been done on several samples and over a period of time of four months for a same sample.

Routine PXRD. Routine powder X-ray diffraction was carried out on a Bruker D8 Advance A25 diffractometer using Cu Kα radiation equipped with a 1-dimensional position-sensitive detector (Bruker LynxEye). X-ray scattering was recorded between 4° and 90° (2θ) with 0.02° steps and 0.5 s per step (28 min for the scan). Divergence slit was fixed to 0.2° and the detector aperture to 189 channels (2.9°).

SEM. SEM images were obtained with FEI Quanta 250 FEG scanning electron microscope. Samples were mounted on stainless pads and sputtered with carbon to prevent charging during observation.

FT-IR. The infrared spectra were obtained from a Bruker Vector 22 FT-IR spectrometer with KBr pellets at room temperature and registered from 4000 cm^{-1} to 400 cm^{-1}.

TGA. Thermo-gravimetric analyses (TGA) were performed with a TGA/DSC 1 STARe System from Mettler Toledo. Around 2 mg of sample was heated at a rate of 10 °C.min^{-1}, in a 70 μL alumina crucible, under argon atmosphere (20 mL.min^{-1}). The final product is Cu_2S (59.4 wt%).

XPS. The XPS spectra were recorded with a CLAM 4 vacuum generator (Mg Kα line at 1253.6 eV), and the photoelectrons were collected at a pass energy of 20 eV (energy step of 0.1 eV) in the fixed analyzer transmission mode. The sample (sintered pellet with a diameter of 3 mm) was mounted on a pin raised by few mm from the support plate to avoid contamination from the support. Preliminary to the XPS measurements, a soft argon sputtering was performed in order to clean the surface and improve the signal (the sputtering conditions have been optimized so as not to deteriorate the sample). Spectra were analyzed using CasaXPS software. GL(20) profiles and Shirley-type background were used for each component.[1] Typical XPS energy spectrum recorded over the Cu2p core level energy range is shown in the Figure S6. The dominant signal comes from the Cu(I) (as confirmed by the Auger parameter found at 1849 eV typical for the Cu(I) 2p3/2), core levels Cu(2p3/2) and Cu(2p1/2) obtained at binding energies of 932.8 eV and 952.6 eV respectively. A contribution from the Cu(II)-2p core levels is observed with the typical Cu(II) shake-up satellite at 944.2 eV.[2] In average, the fits lead to a ratio of 0.8Cu(I) and 0.2Cu(II).

UV-vis. UV-vis absorption spectrum was carried out with a LAMBDA 365 UV/Vis Spectrophotometer from Perkin Elmer in solid state with KBr at room temperature. The Figure S7 left is obtained with Planck-Einstein formula and the Figure S7 right is obtained according to the Tauc's equation based on UV-Vis spectra with $\gamma = \frac{1}{2}$ for direct bandgap.[3]

Structure resolution. High resolution X-ray powder diffraction data were collected on the CRISTAL beamline at Soleil Synchrotron (Gif-sur-Yvette, France). A monochromatic beam was extracted from the U20 undulator beam by means of a Si(111) double monochromator. Its wavelength of 0.72844 Å was refined from a LaB6 (NIST Standard Reference Material 660a) powder diagram recorded prior to the experiment. The sample was loaded in a 0.7 mm capillary (Borokapillaren, GLAS, Schönwalde, Germany) mounted on a spinner rotating at

about 5 Hz to improve the particles' statistics. Diffraction data were collected in continuous scanning mode with a MYTHEN2 X 9K detector (Dectris) allowing a measurement in less than 5 minutes. Calculations of structural investigations were performed with the TOPAS (indexing and Rietveld refinement),[4] and FOX (simulated annealing) programs. The LSI-indexing method converged to a monoclinic unit cell with satisfactory figures of Merit (see table S1). Systematic extinctions were consistent with the $P2_1/c$ space group, which was used to initialize the structural determination. Simulated annealing process led us to locate, in general positions, the two independent copper atoms as well as the 1,3-benzenedithiolate molecule which was treated as rigid body. The final Rietveld plot (Fig. S4), corresponds to satisfactory model indicator and profile factors (Table S2). This involves 18 structural parameters: 1 scale factor, 6 atomic coordinates for Cu atoms, 6 parameters for the orientation and the translation of the organic moiety, 2 distances and 2 angles inside the rigid body and 1 overall temperature factor.

Formation of pellets and density measurements. A mechanical press is used for the formation of pellets for conductivity experiments. Between 30-50 mg of crushed powder sample is introduced in a sample chamber. Then a pressure of 0.6 MPa is applied for 15 minutes. The diameter of the pellets is 4 mm and the thickness 1 mm. The density of the pellet is measured by using the Archimedes' principle in absolute ethanol. The measured density is 2.24, considering theoretical density of $[Cu_2(1,3\text{-BDT})]_n$ from crystallographic data of 2.64, the densification of the pellet is 85 %. The pressed pellets were stored for several weeks under atmospheric conditions without any decomposition.

Electrical properties using the four point probe method. The electrical resitivity is measured by means of a Keithley 2450 sourcemeter instrument associated with a linear array of four needle–like electrodes arranged linearly with equidistant spacing between the probes (from Jandel). The four probes are made of tungsten carbide (300 µm in diameter) and have a 500 µm spacing. The outer two electrodes into the material inject a current and the two inner electrodes measure the resulting electric potential distribution. With such distribution, current injection and determination of electric potential using separate electrodes, the measured results will not include the contact resistance between the metal electrodes and the sample/material. The applied force on the probes was controlled and monitored around 60 g (corresponding to a force of about 590 mN) via a force gauge placed under the sample

holder. I-V measurements were recorded from which the resistance (R) was extracted by using a linear fit in the range where it behaves linearly (Fig. S8). For $[Cu_2(1,3\text{-BDT})]_n$, this resistance is R = 3 kΩ.

Then, in the 4-probes method for 3D-bulk sample, the material resistivity (ρ) is given by:[5]

$$\rho = R * 2\pi * S$$

with R, the resistance obtained from the Ohm's law and S, the distance between the electrodes (S = 635 µm).

Seebeck experiment: Seebeck coefficient (S) was measured using the differential method S = ΔV/ΔT (Figure below), where ΔV is the thermoelectromotive force induced by the thermal gradient ΔT, in a high-temperature setup, similar to that described in previous work.[6] Measurement was performed under primary vacuum (10^{-1} mBar) at different temperatures slightly above room temperature (Figure S14).

DFT simulations. DFT calculations were performed using the Vienna ab initio Simulation Package (VASP) version 5.4,[7] with projector-augmented wave function (PAW) pseudopotentials[8] and the Perdew-Burke-Ernzerhof exchange-correlation functional (PBE).[9] A planewave cutoff of 400 eV and an electron density convergence criteria of 10-6 eV were found to yield converged results. The Brillouin Zone was sampled with a 4 × 8 × 2 Monkhorst-Pack mesh reflecting the asymmetrical unit cell of the system. Starting from the experimental X-ray structure, the atomic positions were relaxed until the energetical change was less than 10-3 eV. The unit cell was kept fixed during this process. The electronic density of states was computed using a finer Gamma-centered 10 x 20 x 5 Monkhorst-Pack mesh and visualized with the PyProcar software. The Seebeck coefficient was computed using BoltzTraP2 based on the band structure computed by VASP.

Table S1. Room temperature thermoelectric properties of reported MOFs/CPs and $[Cu_2(1,3\text{-}BDT)]_n$: σ, the electric conductivity; S, the Seebeck coefficient; PF, the power factor; κ, the thermal conductivity and ZT the figure of merit. In darker, the best values.

MOFs/CPs	Structure	σ ($S.cm^{-1}$)	S ($\mu V.K^{-1}$)	PF ($\mu W.m^{-1}.K^{-2}$)	κ ($W.m^{-1}.K^{-1}$)	ZT	ref
Cu_X(BHT)	2D	**2000**	-21	88.2	1.99	0.013	[10]
Cu_4(BHT)	2D	270	40	40	0.72	0.02	[11]
$Cu_{5.5}$(BHT)	2D	220	80	**140**	0.59	**0.08**	[11]
$Ni_3(HITP)_2$	2D and porous	58.8	-11.9	0.833	**0.21**	$1.19.10^{-3}$	[12]
Ni-PTC	2D	9	47	1.988	**0.20**	0.003	[13]
Zn-HAB	3D and porous	$0.86.10^{-3}$	200	$3.44.10^{-3}$	-	-	[14]
$Cu_3(HHTP)_2$	2D and porous	$2.28.10^{-3}$	-121.4	$3.15.10^{-3}$	-	-	[15]
$[Cu_2(1,3\text{-}BDT)]_n$	2D	$1.5.10^{-3}$	**420**	0.026			*This work*

BHT: benzenehexathiolate, HITP: 2,3,6,7,10,11-hexaiminotriphenylene, PTC: 1,2,3,4,5,6,7,8,9,10,11,12-Perthiolated coronene, HAB: hexaaminobenzene, HHTP: 2,3,6,7,10,11-hexahydroxytriphenylene.

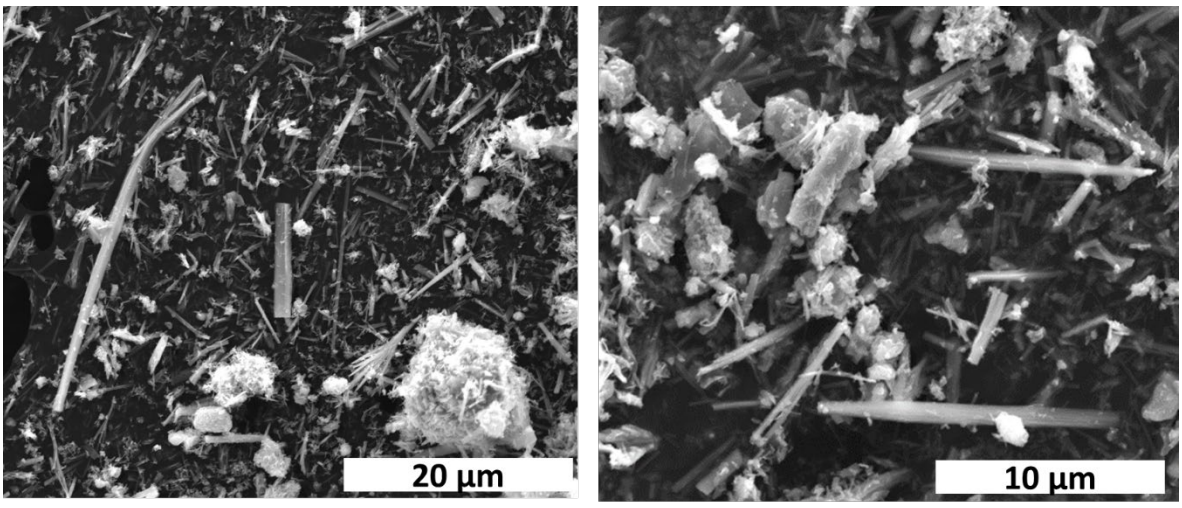

Figure S1. Scanning electron microscopy images of $[Cu_2(1,3\text{-}BDT)]_n$.

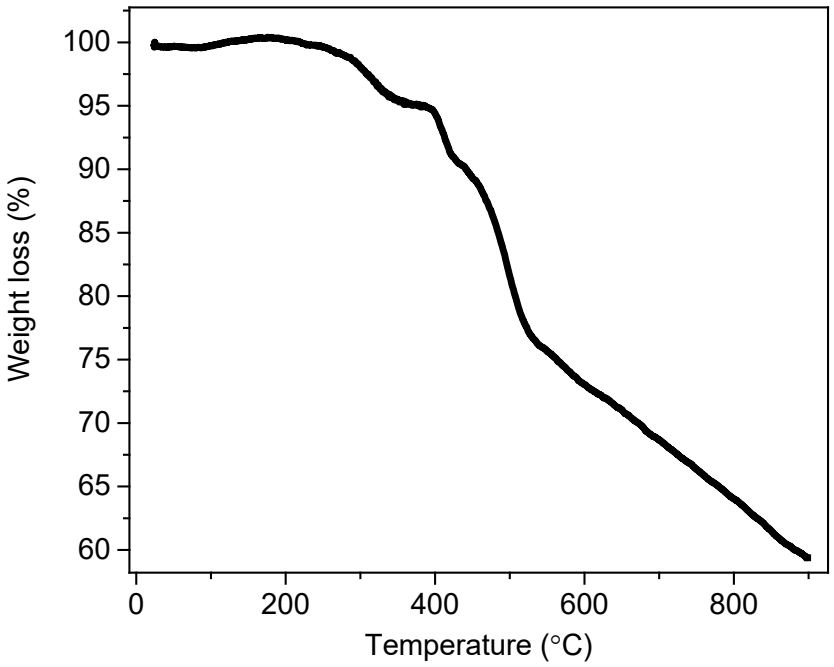

Figure S2. Thermo-gravimetric analysis of $[Cu_2(1,3\text{-BDT})]_n$ carried out under argon at 10 ˚C/min.

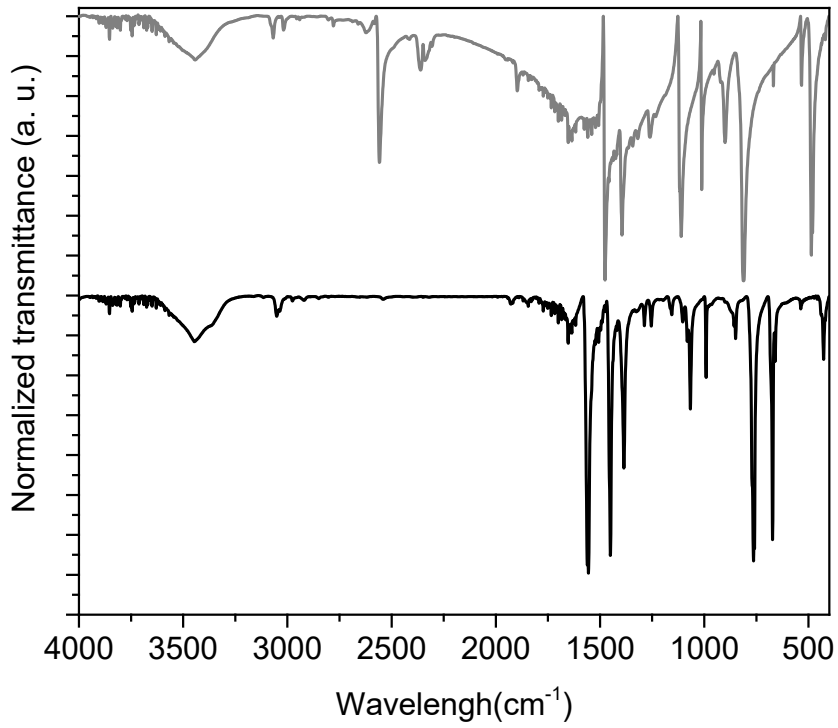

Figure S3. FT-IR spectra of $[Cu_2(1,3\text{-BDT})]_n$ (black) and the ligand 1,3-H2BDT (grey).

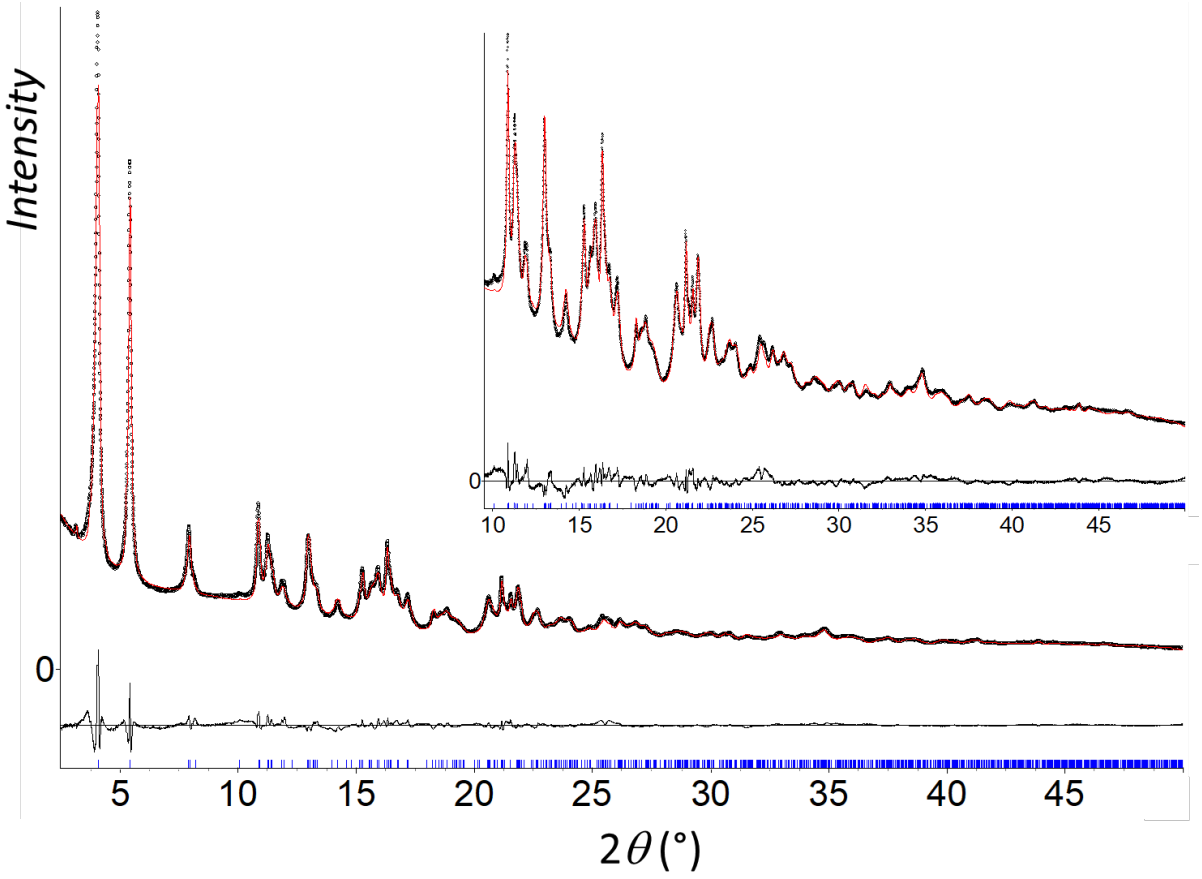

Figure S4. Final Rietveld plot of $[Cu_2(1,3\text{-BDT})]_n$ showing observed (black dotes), calculated (red line), and difference (black line) curves (λ = 0.72844 Å). A zoom is shown as inset.

Table S2. Crystallographic data and Rietveld refinement parameters for $[Cu_2(1,3\text{-BDT})]_n$.

Empirical formula	$C_6H_5Cu_2$
M_r	267.32
Crystal system	Monoclinic
Space group	$P2_1/c$
a (Å)	10.981(2)
b (Å)	3.9726(5)
c (Å)	16.592(2)
β (°)	111.824(7)
V (Å^3)	671.9 (2)
d	2.642
M_{20}	13
Z	4
λ (Å)	0.72844
No of structural	18
Number of reflections	1133
R_p, R_{wp}	0.028, 0.032
R_{Bragg}, *GoF*	0.015, 4.95

a.

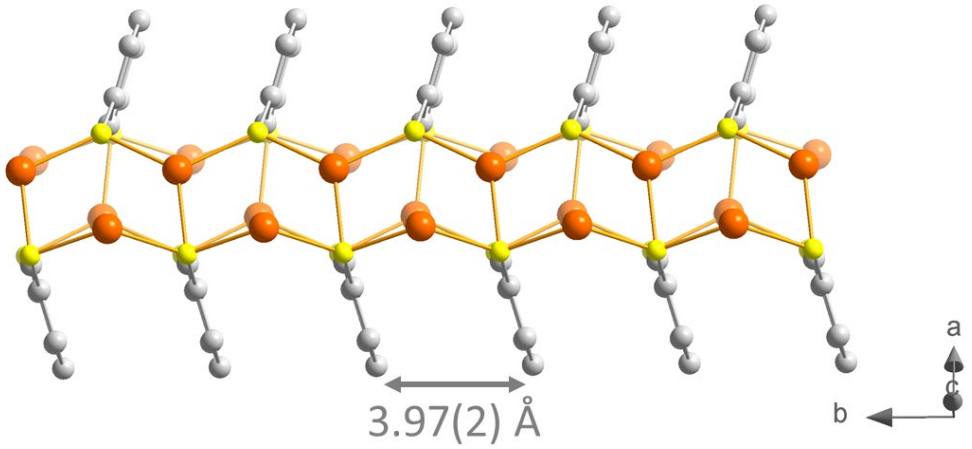

b.

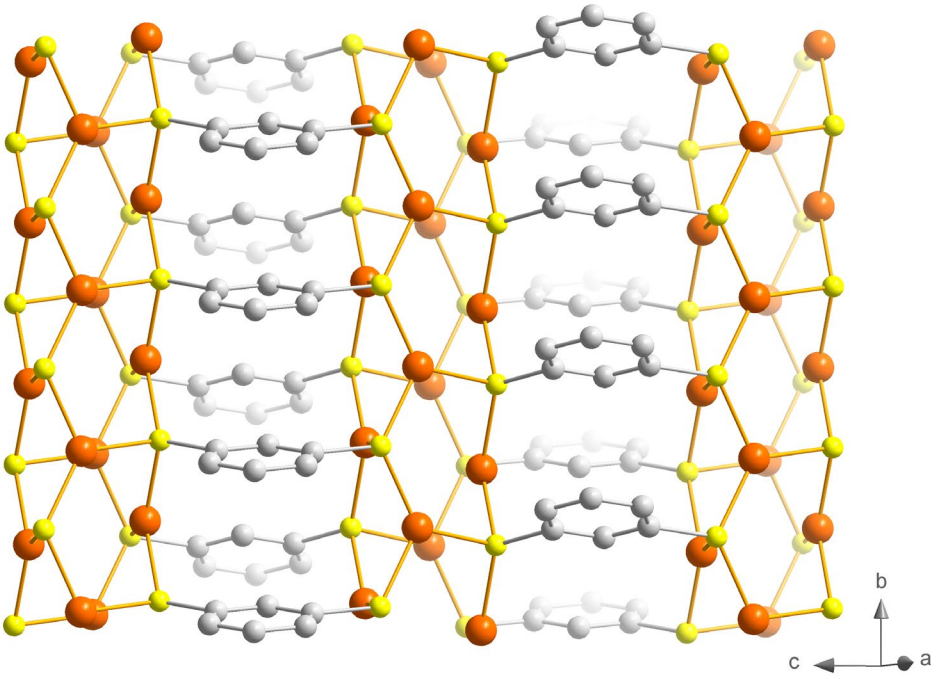

c.

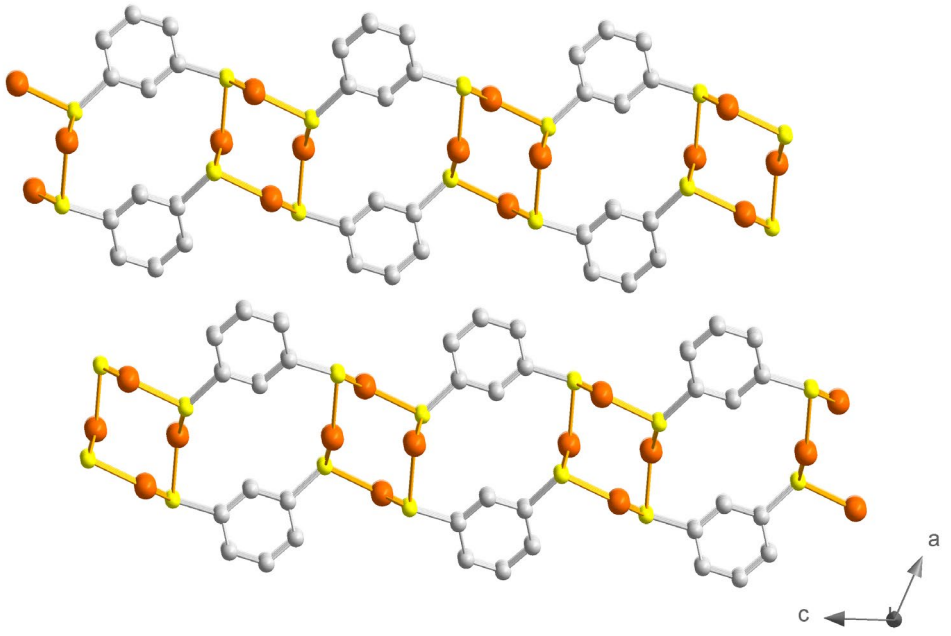

Figure S5. Representations of the structure of $[Cu_2(1,3\text{-BDT})]_n$: a. view of the chains along the *b* axis, the distance between the aromatic rings shows the absence of π-π interaction,[16] b. view of chains bridged by the ligands and c. view of the packing of the chains. Orange, yellow and gray spheres correspond to copper, sulfur and carbon atoms. Hydrogen atoms were omitted for clarity.

Table S3. Selected bonds and angles of $[Cu_2(1,3\text{-BDT})]_n$.

Cu-S (Å)	Cu2-S2: 2.20(2), 2.29(2) Cu1-S1: 2.24 (2), 2.26(2) Cu2-S1: 2.24 (2) Cu1-S2: 2.26(2)
Cu-Cu (Å)†	Cu2 – Cu2: 2.947 (4) Å Cu1 – Cu1: 3.797 (3) Å
Cu-S-Cu (°)	Cu1-S1-Cu2: 75.0(7), 85.3(7) Cu1-S2-Cu2: 87(1), 103(1) Cu1-S1-Cu1: 123.7(7) Cu2-S2-Cu2: 125(1)
S-Cu-S (°)	S1-Cu1-S2: 109.1(7), 127.2(8) S2-Cu2-S1: 110.9(8), 123.6(8) S1-Cu1-S1: 123.7(6) S2-Cu2-S2: 124.5(9)

† Copper ions not bridged by sulfur atoms.

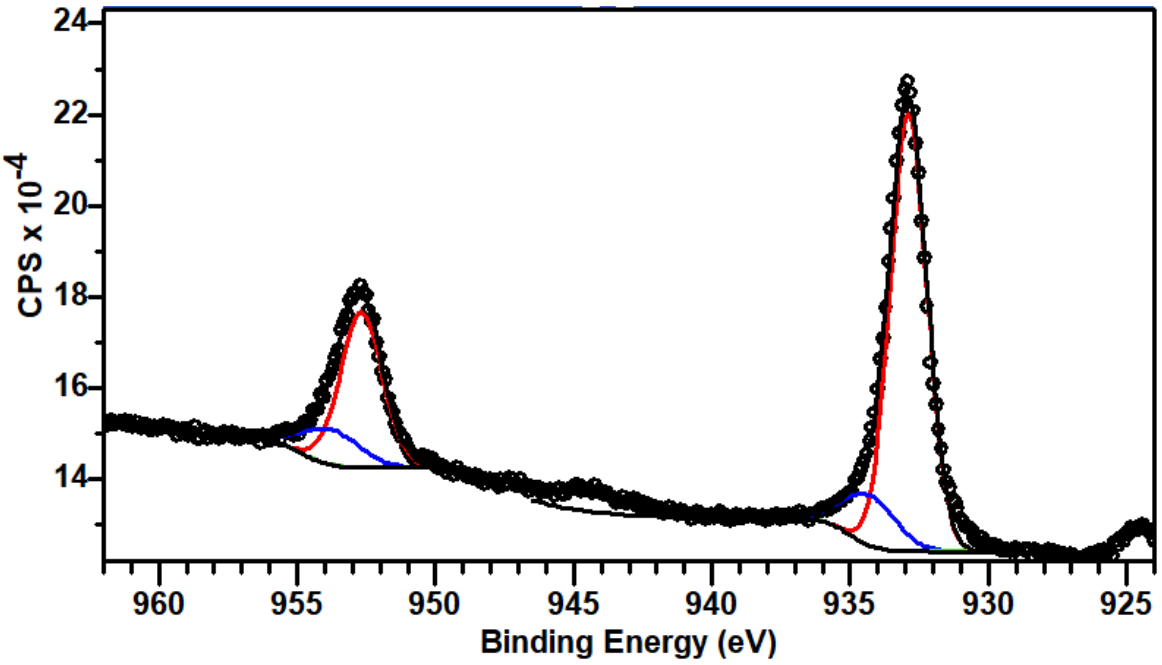

Figure S6. Measured Cu 2p XPS spectrum of $[Cu_2(1,3\text{-BDT})]_n$ (opened circles) The colored lines show the fitting profiles of Cu(+I) (red) and Cu(+II) (blue). The small amount of Cu(II) oxidation state, can be seen by a typical shake-up structure at 944.2 eV and may be due to partial decomposition at the surface or impurities from the sample

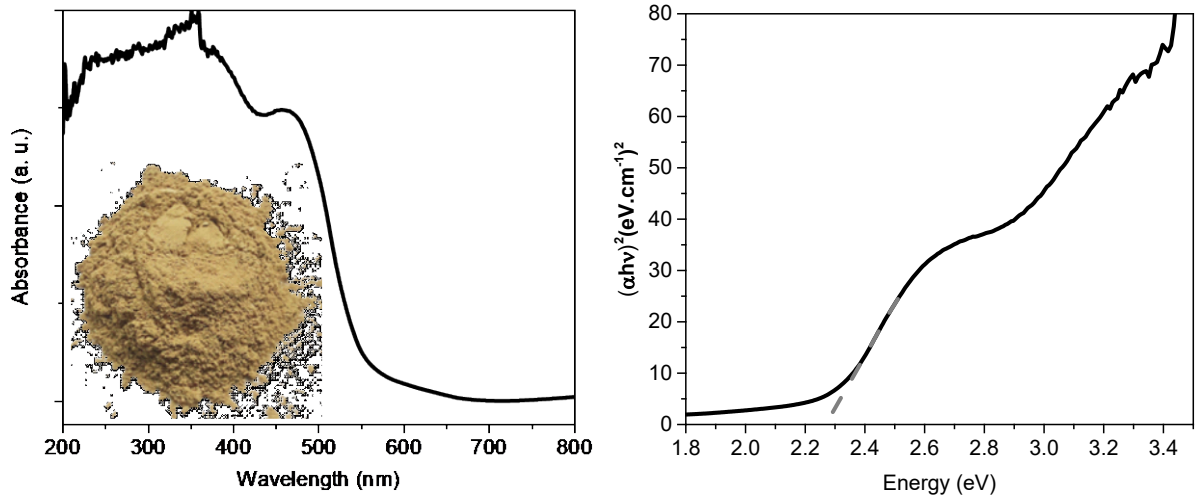

Figure S7. UV-visible spectrum (left) of $[Cu_2(1,3\text{-BDT})]_n$ with a photo of the powder as inset and the evaluation of its direct bandgap by Tauc plot (right).

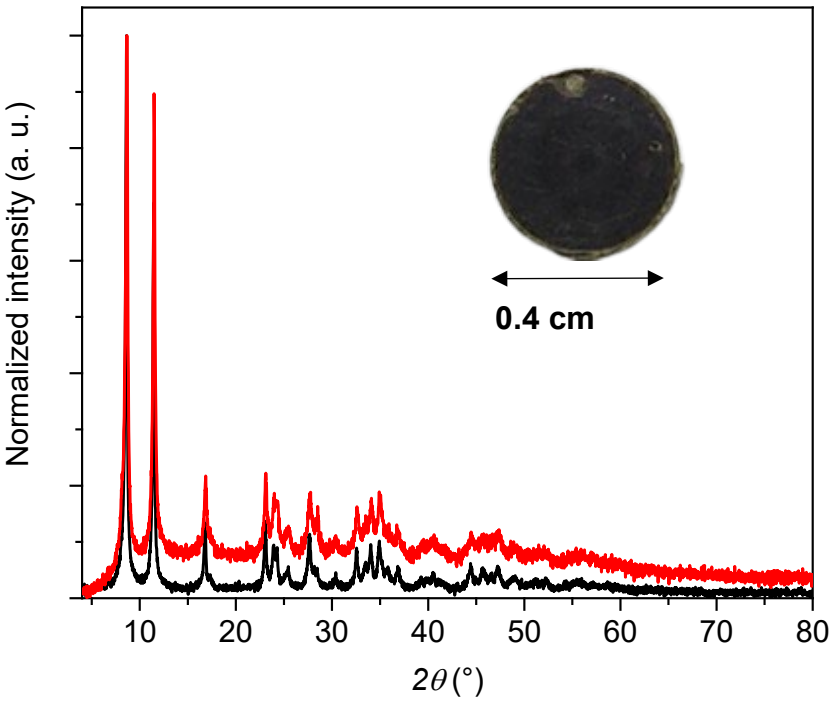

Figure S8. Powder XRD data (λ = 1.5406 Å) of $[Cu_2(1,3\text{-BDT})]_n$ as it was freshly synthesized (black) and after (red) the formation of the pellet which has been hand crushed four months after its synthesis to get a powder before measurement. Inset, a photo of a $[Cu_2(1,3\text{-BDT})]_n$ pellet.

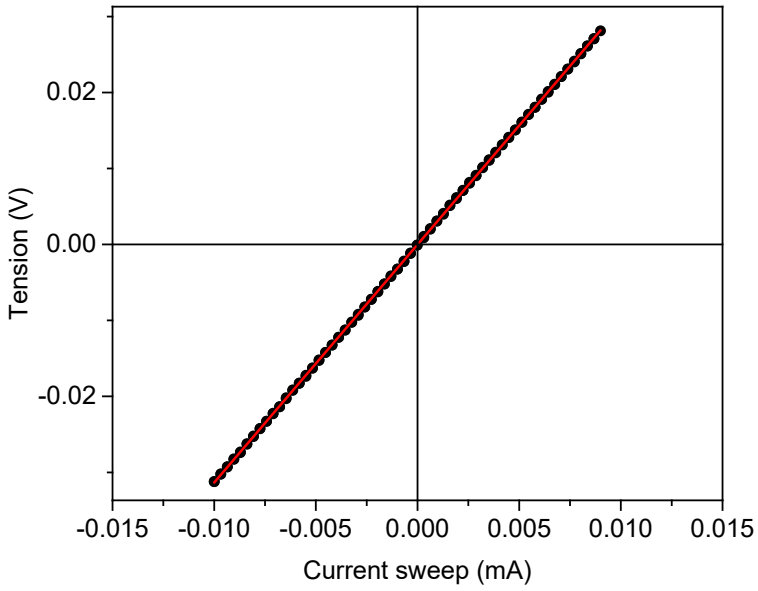

Figure S9. Four probe Current-Voltage (I-V) measurement on a pressed pellet of $[Cu_2(1,3\text{-}BDT)]_n$ at RT. The resistance obtained from the linear fit is R = 3 kΩ. The linear fit of the data (red line) reveals a conductivity of $8.35.10^{-4}$ S/cm.

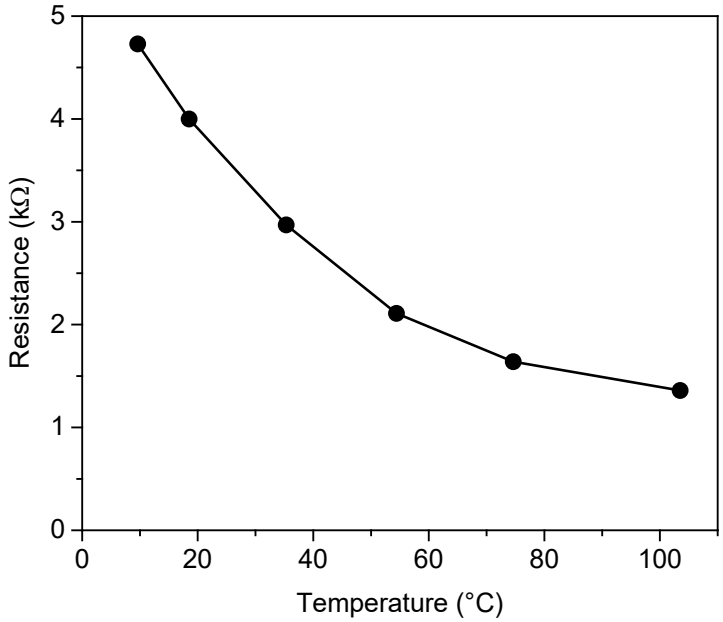

Figure S10. Resistance temperature dependence by surface four-probe configuration on a pressed pellet of $[Cu_2(1,3\text{-}BDT)]_n$.

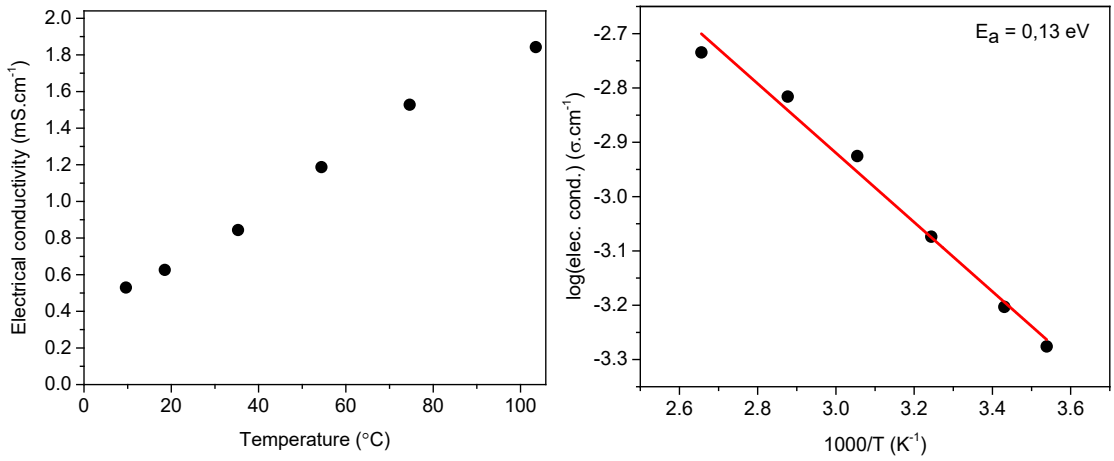

Figure S11. Temperature dependence of the electrical conductivity measured on the $[Cu_2(1,3\text{-}BDT)]_n$ pellet by surface four probe method (left). The Arrhenius plot between 10 and 100 °C gives E_a = 0.13 eV. Arrhenius equation: $\sigma = \sigma_0 \exp(-E_a/k_BT)$, where σ is the electrical conductivity, σ_0 is a prefactor, k_B is the Boltzmann constant, and T is the absolute temperature (right).[17]

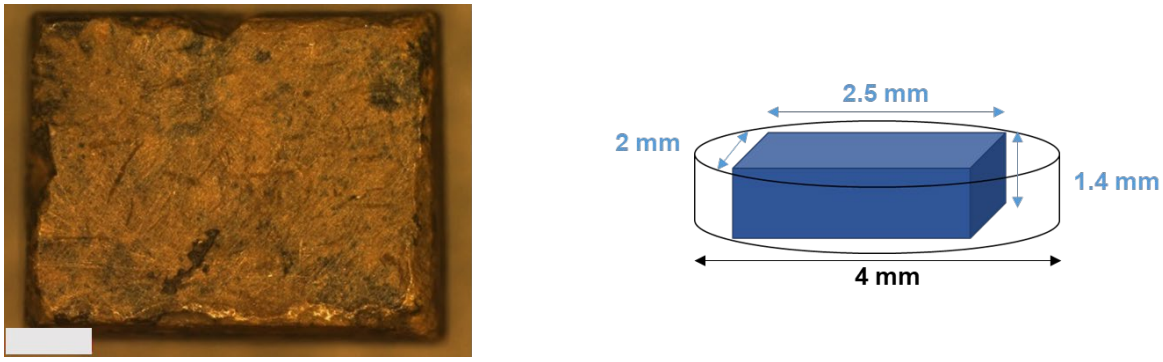

Figure S12. Optical image of the rectangular cuboid of $[Cu_2(1,3\text{-}BDT)]_n$ obtained after cutting the pressed pellet with a corded saw (left), the scale bare is 500 µm, and scheme of its dimensions (right).

a.

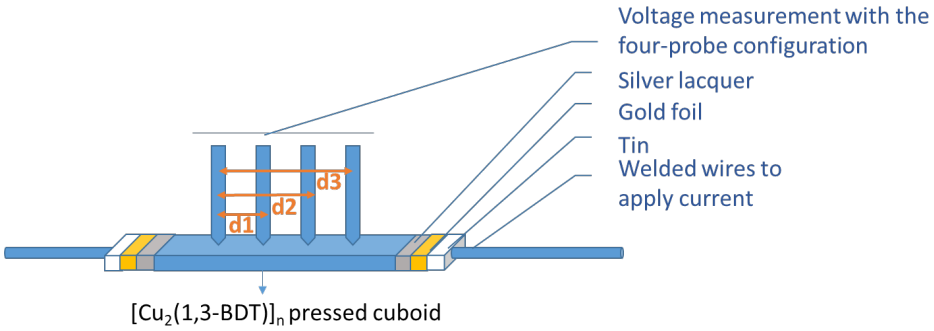

b.

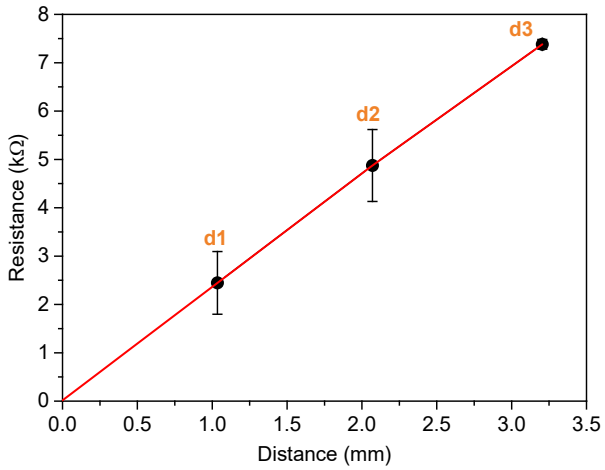

Figure S13. a. Scheme of the setup of the transfer length method (TLM) measurement and b. measurement of the resistance on the pressed cuboid of $[Cu_2(1,3\text{-BDT})]_n$ with the distances (d1, d2 and d3) between the electrodes of the four-probe configuration. The linear fit in red gives a contact resistance R_c = 0.017 kΩ.

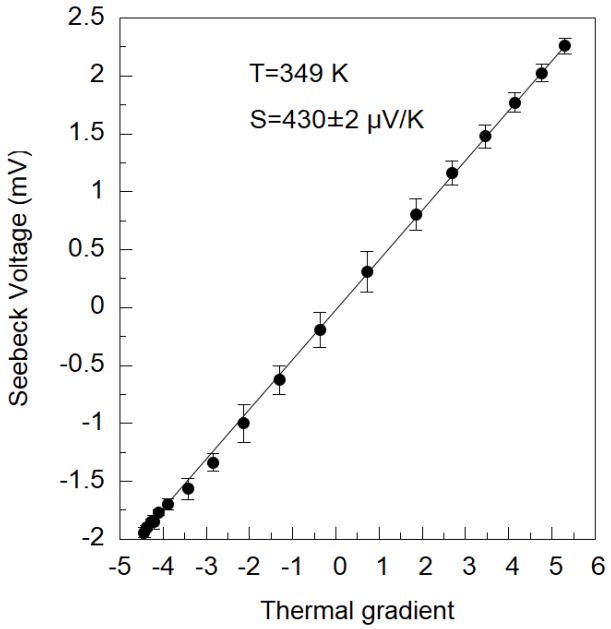

Figure S14. Measured thermal voltage as a function of the applied thermal gradient measured at an average temperature of about 350 K (black filled points). The Seebeck (S) is extracted from a linear fit (black line).[6]

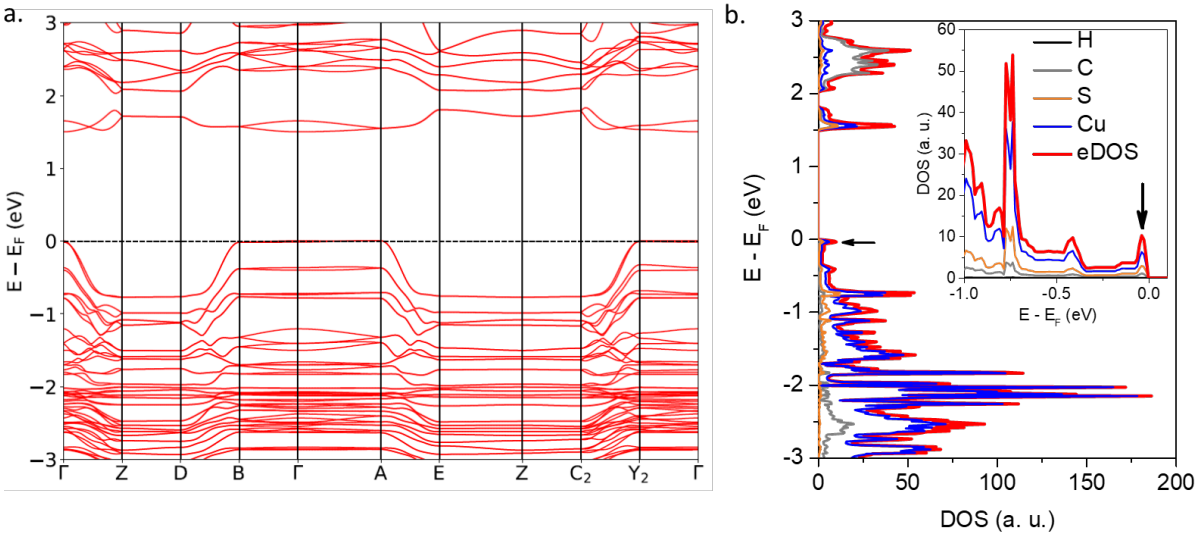

Figure S15. a. Calculated band structure along the main symmetry direction in the reciprocal space in $[Cu_2(1,3\text{-BDT})]_n$. The Femi level (dotted line) is fixed to be at the edge of the valence band b. Density of states (DOS) of $[Cu_2(1,3\text{-BDT})]_n$: projected electronic DOS (p-eDOS) with grey line for C, black for H, orange for S and blue for Cu electrons and the total electronic DOS (eDOS) in red. The insert is a zoom close to the Fermi level and with switched axes. The black arrows show the shard peaks associated to high Seebeck coefficient.

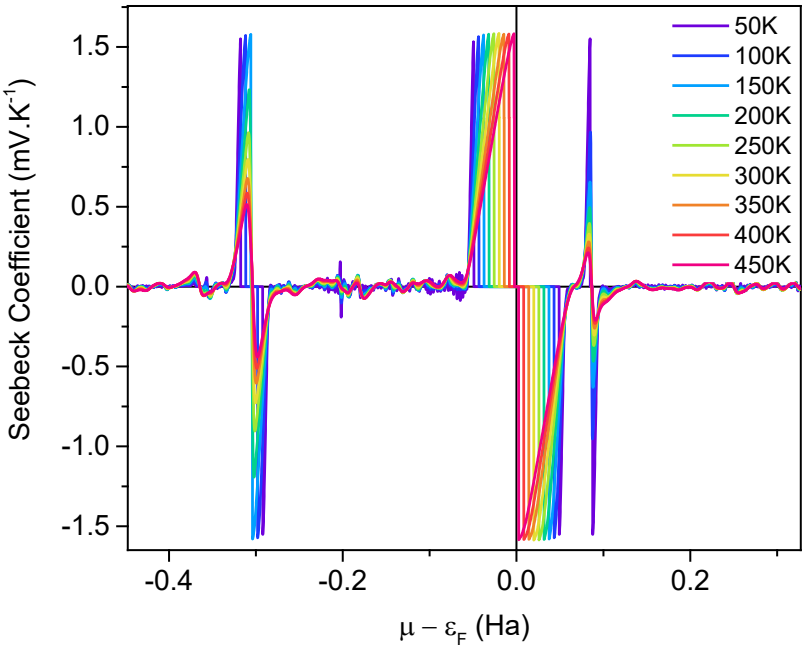

Figure S16. Calculated Seebeck coefficients at different temperatures.

REFERENCES

1. Fairley, N., http://www.casaxps.com, © Casa software Ltd. 2005.

2. Biesinger, M. C., Advanced analysis of copper X-ray photoelectron spectra. *Surf. Interface Anal.* **2017,** *49*, 1325.

3. Makuła, P.; Pacia, M.; Macyk, W., How To Correctly Determine the Band Gap Energy of Modified Semiconductor Photocatalysts Based on UV–Vis Spectra. *J. Phys. Chem. Lett.* **2018,** *9*, 6814.

4. *Topas V5.0: General Profile and Structure Analysis Software for Powder Diffraction Data, Bruker AXS Ltd,* ***2014****.*

5. Miccoli, I.; Edler, F.; Pfnür, H.; Tegenkamp, C., The 100th anniversary of the four-point probe technique: the role of probe geometries in isotropic and anisotropic systems. *J. Phys.: Condens. Matter* **2015,** *27*, 223201.

6. (a) Han, D.; Moalla, R.; Fina, I.; Giordano, V. M.; d'Esperonnat, M.; Botella, C.; Grenet, G.; Debord, R.; Pailhès, S.; Saint-Girons, G.; Bachelet, R., Giant Tuning of Electronic and Thermoelectric Properties by Epitaxial Strain in p-Type Sr-Doped LaCrO3 Transparent Thin Films. *ACS Appl. Electron. Mater.* **2021,** *3*, 3461; (b) Rouleau, O.; Alleno, E., Measurement system of the Seebeck coefficient or of the electrical resistivity at high temperature. *Review of Scientific Instruments* **2013,** *84*, 105103.

7. (a) Kresse, G.; Hafner, J., Ab initio molecular dynamics for liquid metals. *Phys. Rev. B* **1993,** *47*, 558; (b) Kresse, G.; Hafner, J., Ab initio molecular-dynamics simulation of the liquid-metal--amorphous-semiconductor transition in germanium. *Phys. Rev. B* **1994,** *49*, 14251; (c) Kresse, G.; Furthmüller, J., Efficient iterative schemes for ab initio total-energy calculations using a plane-wave basis set. *Phys. Rev. B* **1996,** *54*, 11169.

8. (a) Blöchl, P. E., Projector augmented-wave method. *Phys. Rev. B* **1994,** *50*, 17953; (b) Kresse, G.; Joubert, D., From ultrasoft pseudopotentials to the projector augmented-wave method. *Phys. Rev. B* **1999,** *59*, 1758.

9. Perdew, J. P.; Burke, K.; Ernzerhof, M., Generalized Gradient Approximation Made Simple. *Phys. Rev. Lett.* **1996,** *77*, 3865.

10. Tsuchikawa, R.; Lotfizadeh, N.; Lahiri, N.; Liu, S.; Lach, M.; Slam, C.; Louie, J.; Deshpande, V. V., Unique Thermoelectric Properties Induced by Intrinsic Nanostructuring in a Polycrystalline Thin-Film Two-Dimensional Metal–Organic Framework, Copper Benzenehexathiol. *Phys. Status Solidi A* **2020,** *217*, 2000437.

11. Huang, X.; Qiu, Y.; Wang, Y.; Liu, L.; Wu, X.; Liang, Y.; Cui, Y.; Sun, Y.; Zou, Y.; Zhu, J.; Fang, W.; Sun, J.; Xu, W.; Zhu, D., Highly Conducting Organic–Inorganic Hybrid Copper Sulfides CuxC6S6 (x=4 or 5.5): Ligand-Based Oxidation-Induced Chemical and Electronic Structure Modulation. *Angew. Chem. Int. Ed.* **2020,** *59*, 22602.

12. Sun, L.; Liao, B.; Sheberla, D.; Kraemer, D.; Zhou, J.; Stach, E. A.; Zakharov, D.; Stavila, V.; Talin, A. A.; Ge, Y.; Allendorf, M. D.; Chen, G.; Léonard, F.; Dincă, M., A Microporous and Naturally Nanostructured Thermoelectric Metal-Organic Framework with Ultralow Thermal Conductivity. *Joule* **2017,** *1*, 168.

13. Chen, Z.; Cui, Y.; Jin, Y.; Liu, L.; Yan, J.; Sun, Y.; Zou, Y.; Sun, Y.; Xu, W.; Zhu, D., Nanorods of a novel highly conductive 2D metal–organic framework based on perthiolated coronene for thermoelectric conversion. *J. Mater. Chem. C* **2020,** *8*, 8199.

14. Park, J.; Hinckley, A. C.; Huang, Z.; Chen, G.; Yakovenko, A. A.; Zou, X.; Bao, Z., High Thermopower in a Zn-Based 3D Semiconductive Metal–Organic Framework. *J. Am. Chem. Soc.* **2020,** *142*, 20531.

15. de Lourdes Gonzalez-Juarez, M.; Flores, E.; Martin-Gonzalez, M.; Nandhakumar, I.; Bradshaw, D., Electrochemical deposition and thermoelectric characterisation of a semiconducting 2-D metal–organic framework thin film. *J. Mater. Chem. A* **2020,** *8*, 13197.

16. Martinez, C. R.; Iverson, B. L., Rethinking the term “pi-stacking”. *Chem. Sci.* **2012,** *3*, 2191.

17. Sun, L.; Campbell, M. G.; Dincă, M., Electrically Conductive Porous Metal–Organic Frameworks. *Angew. Chem. Int. Ed.* **2016,** *55*, 3566.